SCIENTIFIC REPORTS

OPEN

SUBJECT AREAS:
CELL DEATH
PERMEATION AND TRANSPORT

Received
2 October 2014

Accepted
19 December 2014

Published
26 January 2015

Correspondence and requests for materials should be addressed to F.J.P.K. (fkuehn@physiology.rwth-aachen.de)

Functional Characterisation of a TRPM2 orthologue from the sea anemone *Nematostella vectensis* in human cells

Frank J. P. Kühn, Cornelia Kühn & Andreas Lückhoff

Institute of Physiology, Medical Faculty, RWTH Aachen, D52057 Aachen, Germany.

The human non-selective cation channel TRPM2 represents a mediator of apoptosis triggered by oxidative stress. The principal agonist ADP-ribose binds to the cytosolic domain of TRPM2, which is homologous to the human ADP-ribose pyrophosphatase NUDT9. To further elucidate the structure-function relationship of this channel, we characterised a TRPM2 orthologue from the cnidarian *Nematostella vectensis*, after its expression in a human cell line. This far distant relative shows only 31% total sequence similarity to *h*TRPM2, while its C-terminal domain has a greater resemblance to the NUDT9 enzyme. Current through *nv*TRPM2 was induced by ADPR, with a more pronounced sensitivity and faster kinetics than in *h*TRPM2. In contrast to *h*TRPM2, there was no response to H_2O_2 and hardly any modulatory effect by intracellular Ca^{2+}. The deletion of a stretch of 15 residues from the NUDT9 domain of *nv*TRPM2, which is absent in *h*TRPM2, did not change the response to ADPR but enabled activation of the channel by H_2O_2 and increased the effects of intracellular Ca^{2+}. These findings shed new light on the evolution of TRPM2 and establish *nv*TRPM2 as a promising tool to decipher its complex gating mechanisms.

The transient receptor potential (TRP) subfamily of tetrameric cation channels contains various members with unusual properties, most notably TRPM2 with its integrated enzyme domain[1]. The C-terminal region of TRPM2 is homologous to the human (*h*) enzyme NUDT9 which represents an adenosine 5′-diphosphoribose (ADPR) pyrophosphatase of the NUDIX hydrolase family[2]. Channel gating most likely requires the binding but not the cleavage of the principal agonist ADPR (EC_{50} of approximately 100 μM)[1] because the NUDT9 domain of TRPM2 contains mutations essential for channel function that reduce the ADPRase activity of the *h*NUDT9 enzyme by two orders of magnitude[3–5]. Cellular ADPR is produced by NAD^+ metabolising enzymes on the plasma membrane such as CD38 which also hydrolyses cyclic ADPR to ADPR[6]. During apoptosis the release of ADPR into the cytosol is also driven by the poly-ADPR polymerase (PARP) and poly-ADPR glycohydrolase (PARG) pathways[7,8]. Numerous experimental data have assigned an important physiological role for TRPM2 in type I and type II diabetes, inflammation, lysosomal Ca^{2+} release as well as in cardiovascular and neurodegenerative diseases that are closely associated with apoptosis (for reviews see refs 9, 10). Currently, the most accepted hypothesis for the stimulation of TRPM2 by oxidative stress is that oxidants induce the accumulation of intracellular ADPR, which in turn activates TRPM2[5]. As an experimental model for oxidative stress, extracellular H_2O_2 is frequently utilised and has been shown to trigger TRPM2 activation[11,12]. There is a positive Ca^{2+}-driven feedback loop during the activation of TRPM2 because Ca^{2+} entry through the channel pore sensitises TRPM2 to the activation by ADPR[1,13–15], all of which contributes to a fatal increase in the intracellular Ca^{2+} concentration during apoptosis.

Currently, there is little information regarding the structural requirements for the unique activation of TRPM2, mostly due to a lack of adequate experimental strategies to properly address the question. Orthologues of other TRP channels have been successfully exploited to elucidate the widely divergent gating mechanisms within the family (e.g., ref. 16). From phylogenetic analyses, there is evidence that a TRPM2-like channel containing a NUDT9 homology region (NUDT9H) represents the archetypal TRPM channel of non-metazoan origin[17]. This has been concluded because TRPM2-like channels are the only representatives of the TRPM- subfamily in the unicellular choanoflagellate *Monosiga brevicollis* as well as in the cnidarian *Nematostella vectensis*[17]. Currently, *Nematostella vectensis* represents a popular model organism for the evolution of the nervous system[18] and the immune system[19] in which the human TRPM2 channel plays an important physiological role[9,10].

The aim of the present study was the functional analysis of the TRPM2-like channel of *Nematostella vectensis* (*nv*TRPM2) after heterologous expression in a human cell line. Through the generation of channel chimeras

between *nv*TRPM2 and *h*TRPM2, we could gain insight into the functional importance of preserved and altered sections of both channels, particularly into the NUDT9H domain and its relation to channel activation by ADPR, Ca^{2+} and H_2O_2. We report that this approach enables the identification of sequences critical for the response to each stimulus. In addition, our results are the first to provide evidence for a different physiological role of an ADPR-gated cation channel from an organism that is considered as a model system to study early metazoan evolution[20,21].

Results

Heterologous expression of the TRPM2 orthologue. For the functional characterisation *in vitro* of a TRPM2- orthologue far distant from *h*TRPM2, we selected the TRPM2-like channel of the sea anemone *Nematostella vectensis* (jgi.Nemve1.248535|estExt_fgenesh1_pg.C_6220005)[17] the genome of which has been fully sequenced[20] and which is a model organism for comparative studies and development e.g. of the nervous system[18]. We decided for this open reading frame because it yields the maximum sequence coverage and sequence identity, when compared with *h*TRPM2. Furthermore, the culture and manipulation of *Nematostella vectensis* is now established in many laboratorys worldwide, which also enables the implementation of future *in- vivo* studies. Commercially available gene synthesis was used to generate the open reading frame consisting of 4656 base pairs (bp) of the selected *nv*TRPM2 channel (Supplementary Fig. 1) and additionally offers the possibility of modifying the codon usage[22]. Thereby, we ensured the best possible adaption to the mammalian expression system (HEK-293 cells) for our *in- vitro* studies with the TRPM2 orthologue without changing the original sequence of amino acid residues (aa).

Sequence characteristics of the *nv*TRPM2 channel. The selected *nv*TRPM2 channel (1551 aa) displays a total sequence identity of 31% to the *h*TRPM2 channel (1503 aa). The similarity is greatest in the N-terminal region upstream of the putative transmembrane segments (36% identity) and in the NUDT9H domain (39% identity), whereas the regions containing the transmembrane segments (25% identity) and the connecting linker to the NUDT9H domain (27% identity) are less conserved (Supplementary Fig. 2). The NUDT9H domain of *nv*TRPM2 (aa 1271–1551) shows 49% sequence identity to the corresponding sequence of the *h*NUDT9 enzyme (aa 59–350) which is significantly higher than between the *h*NUDT9 enzyme and NUDT9H (aa 1236–1503) of *h*TRPM2 (34%; Supplementary Fig. 3). Compared to the *h*NUDT9-enzyme, in both *nv*TRPM2 and *h*TRPM2, the putative ADPR binding domain[3] of the NUDT9H domain is well conserved, including the critical residue N1326 of *h*TRPM2[4]. However, the active site of the *h*NUDT9 enzyme containing the NUDIX box signature $GX_5EX_7REUXEEXGU$[23] is slightly different in NUDT9H of *nv*TRPM2 and markedly different in NUDT9H of *h*TRPM2 (Supplementary Fig. 3). A short amino acid motif within the proximal part of the predicted pore loop contributes significantly to the Ca^{2+} permeation of TRPM channels[17]. In the non-selective *h*TRPM2 channel, this motif consists of the amino acid triplet glutamine-isoleucine-proline (QIP), whereas in *nv*TRPM2 it is changed to glutamate-leucine-phenylalanine (ELF; Supplementary Fig. 2). Therefore, the *nv*TRPM2 channel contains the signature of a highly Ca^{2+}-permeable channel[17].

As a striking difference to the primary structure of *h*TRPM2, the *nv*TRPM2 channel exhibits a longer S1–S2 linker region with a number of glutamate and lysine residues. Notably, this region shows significant similarity to the corresponding region of the *h*TRPM3 channel (Supplementary Fig. 4), which strengthens the hypothesis that a TRPM2-like channel represents a common ancestor of the contemporary TRPM- subfamily[17].

Sensitivity to ADP-ribose, intracellular and extracellular Ca^{2+} and current kinetics. The functional characterisation of *nv*TRPM2 and *h*TRPM2 transiently expressed in HEK-293 cells was performed with whole-cell patch-clamp analysis and calcium imaging experiments. At moderately increased concentrations of ADPR (25–50 μM) and in the absence of Ca^{2+} ($\leq$10 nM) in the pipette solution, *nv*TRPM2-transfected cells developed large currents immediately after breaking into the cell that returned to baseline within a few seconds (Fig. 1a). The amplitude of these currents was approximately equivalent to the current flow through *h*TRPM2 induced by a 10-fold higher concentration of ADPR (Fig. 1b). As a control, we confirmed that there was no current through *nv*TRPM2 in the absence of ADPR in the pipette solution or when the Ca^{2+}-concentration was buffered to $\leq$10 nM with EGTA on both sides of the cell membrane (Fig. 1c, d), which is also a characteristic feature of *h*TRPM2[13,14]. Accordingly, currents from both *h*TRPM2 and *nv*TRPM2 were elicited in divalent-free extracellular solution only when the ADPR-containing pipette solution was supplemented with 1 μM Ca^{2+} (Fig. 2a).

To quantify the kinetics of inactivation of *nv*TRPM2, we measured the time over which 90% of the current decline occurred, which amounted to 14.1 $\pm$ 4 s (n = 7). This is in striking contrast to *h*TRPM2, which typically shows currents developing slowly and after a characteristic delay, depending on the intracellular concentrations of ADPR and Ca^{2+} (refs 1, 13–15, 24). Moreover, the run-down of *h*TRPM2 currents occurred over several minutes rather than seconds and was frequently incomplete within the time frame of the experiments (Fig. 1b). To assess the kinetics of the current development in *nv*TRPM2 during stimulation with ADPR and without Ca^{2+} in the pipette, experiments were performed in divalent-free extracellular solution (DVF), and currents were initiated by superfusion of the cells with standard bath solution containing 1.2 mM Ca^{2+} (Fig. 1c). Even under these experimental conditions, the activation of *nv*TRPM2 showed no delay, again in distinct contrast to *h*TRPM2[14].

When the pipette solution contained 10 μM ADPR and 1 μM Ca^{2+}, the currents of *nv*TRPM2 were significantly smaller than those observed under conditions in which the patch pipette contained 25 μM ADPR and $\leq$10 nM Ca^{2+} (Fig. 1d). Typically, the ADPR-dependent current development of *h*TRPM2 is accelerated by intracellular Ca^{2+} (e.g. ref. 1). This is demonstrated with experiments shown in Figures 2a and 2b in which currents were either stimulated with 50 μM ADPR and 1 μM Ca^{2+} in the pipette solution (Fig. 2a; extracellular solution divalent free) or with intracelluar 100 μM ADPR and Ca^{2+} buffered to below 10 nM (Fig. 2b; extracellular solution with 1.2 mM Ca^{2+}). In contrast, the current kinetics of *nv*TRPM2 were indistinguishable under both experimental conditions (Fig. 2a, b). These findings suggest that there is no graded modulation by intracellular Ca^{2+} on *nv*TRPM2 under the conditions studied. However, because the characteristic pore motif (ELF) of *nv*TRPM2 indicates a high permeability for Ca^{2+}, the local Ca^{2+} concentration at its proposed activating sites[15] might be considerably higher in *nv*TRPM2 than in *h*TRPM2. Therefore, we generated a *nv*TRPM2 variant with the *h*TRPM2-like pore signature (QLP). This manipulation should reduce the Ca^{2+}-permeability of *nv*TRPM2 to the corresponding level of *h*TRPM2, as others have demonstrated using a similar strategy[17]. The stimulation of *h*TRPM2, *nv*TRPM2 and *nv*TRPM2-(QLP) with 100 μM ADPR and $\leq$10 nM Ca^{2+} in the patch pipette elicited currents with clearly different kinetics (Fig. 2b). In these experiments, the initially divalent-free bath was replaced by a solution containing 1.2 mM Ca^{2+}. In wild-type *nv*TRPM2, this induced an almost instantaneous current activation and a rapid inactivation, whereas the current onset of *h*TRPM2 was strongly delayed. The activation kinetics of the *nv*TRPM2-(QLP) variant were slightly slower compared with wild-type *nv*TRPM2, but were still considerably faster than in *h*TRPM2. The current amplitudes of wild-type *nv*TRPM2 and *nv*TRPM2-

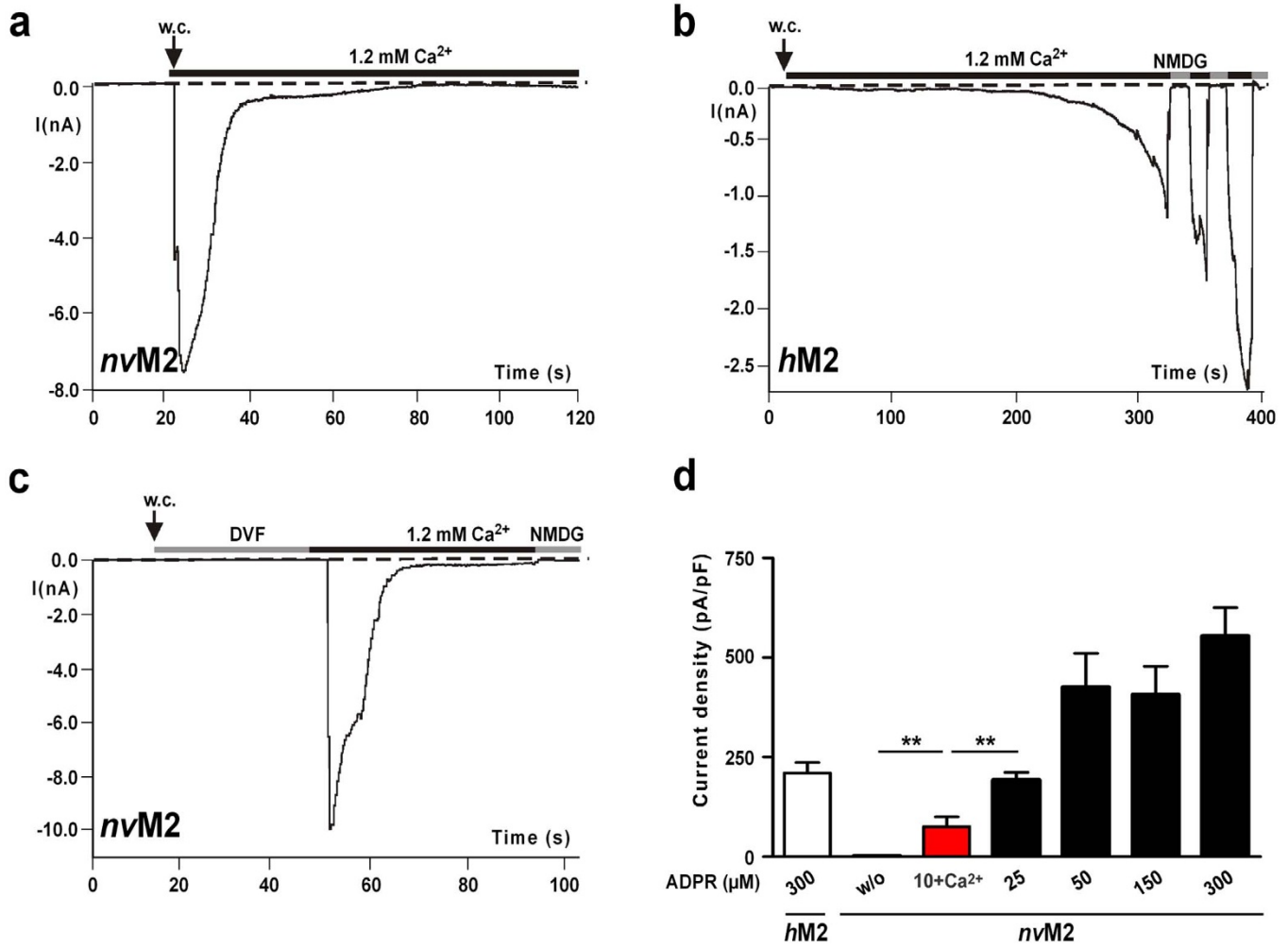

Figure 1 | ADPR-dependent currents of *nv*TRPM2 and *h*TRPM2. (a)–(c) Whole-cell patch-clamp measurements in HEK-293 cells. The pipette solution contained 50 μM ADPR (*nv*TRPM2) or 300 μM ADPR (*h*TRPM2). Intracellular Ca^{2+} concentration was adjusted to ≤10 nM. (a) Instantaneous current development of *nv*TRPM2 after reaching whole-cell configuration (w. c.) in the presence of 1.2 mM extracellular Ca^{2+}. The currents spontaneously and rapidly decline to baseline. (b) Typical slow onset of currents of *h*TRPM2 recorded under the same experimental conditions as in panel a. Repeated current inhibition by substitution of external Na^+ with the impermeable cation NMDG. (c) Same as in panel a, but the whole-cell configuration was established in extracellular divalent-free solution (DVF) in which Ca^{2+} was buffered with EGTA to ≤10 nM. Currents only developed after the extracellular DVF solution was substituted with standard bath solution containing 1.2 mM Ca^{2+}. (D) Current densities in *nv*TRPM2 in dependence on the intracellular ADPR concentration. For experiments with 10 μM ADPR (highlighted in red), the intracellular Ca^{2+}-concentration was adjusted to 1 μM, otherwise the intracellular Ca^{2+}-concentration was below 10 nM. For comparison, corresponding data of *h*TRPM2 at 300 μM ADPR and unstimulated *nv*TRPM2 (w/o) are shown left. **Indicates a significant difference (P = 0.01) from Student's t-test. n = 8–16. Error bars are s.e.

(QLP) evoked with various concentrations of intracellular ADPR (50–300 μM) were not noticeably different.

Therefore, Ca^{2+}-influx through the channel pore of *nv*TRPM2 may accelerate the activation kinetics of the channel. This effect may be explained by yet unidentified Ca^{2+} activating sites near the pore[15]. Both, determination of the relative Ca^{2+} permeability of the QLP variant and the identification of these sites in *nv*TRPM2 and *h*TRPM2 need further experimental investigation.

In our experiments performed with standard bath solution containing 140 mM NaCl, 1.2 mM $CaCl_2$ and 1.2 mM $MgCl_2$, the current-voltage -relationship of wild-type *nv*TRPM2 and *nv*TRPM2-(QLP) displayed a weak double rectification (shown for wild-type *nv*TRPM2 in Fig 2c), in contrast to the strictly linear I/V-curve of *h*TRPM2 (Fig. 2d). The currents reversed at approximately 0 mV and their inward components were inhibited by the replacement of extracellular Na^+ with NMDG (Fig. 2c, d).

Insensitivity of *nv*TRPM2 to oxidative stress induced by the extracellular application of H_2O_2. A key feature of all TRPM2 channel orthologues studied previously is their activation in response to oxidative stress[11,12] that is experimentally simulated by the extracellular application of H_2O_2 (Fig. 2d). Currently the most accepted hypothesis is that H_2O_2 activates the channel indirectly through an accumulation of intracellular ADPR[5]. This view is supported by inside-out patch-clamp experiments in which H_2O_2 apparently had no direct effects on TRPM2[25]. However, a recent study reported that H_2O_2 sensitises *h*TRPM2 to activation by physiological body temperature through the oxidation of a methionine residue localised in the N-terminus of the channel[26]. This specific methionine residue is also conserved in *nv*TRPM2 (Supplementary Fig. 2). Nevertheless, we could not activate *nv*TRPM2 with H_2O_2 even at concentrations of 10–20 mM and in the presence of 1 μM $[Ca^{2+}]_i$ (inset Fig. 2d). Similarly, the variant *nv*TRPM2-(QLP) did not respond to H_2O_2 in either patch-clamp experiments (n = 4) or in calcium imaging experiments (n = 10).

Swapping of the NUDT9 domains of *nv*TRPM2, *h*TRPM2 and the *h*NUDT9 enzyme. To further define the functional role of the

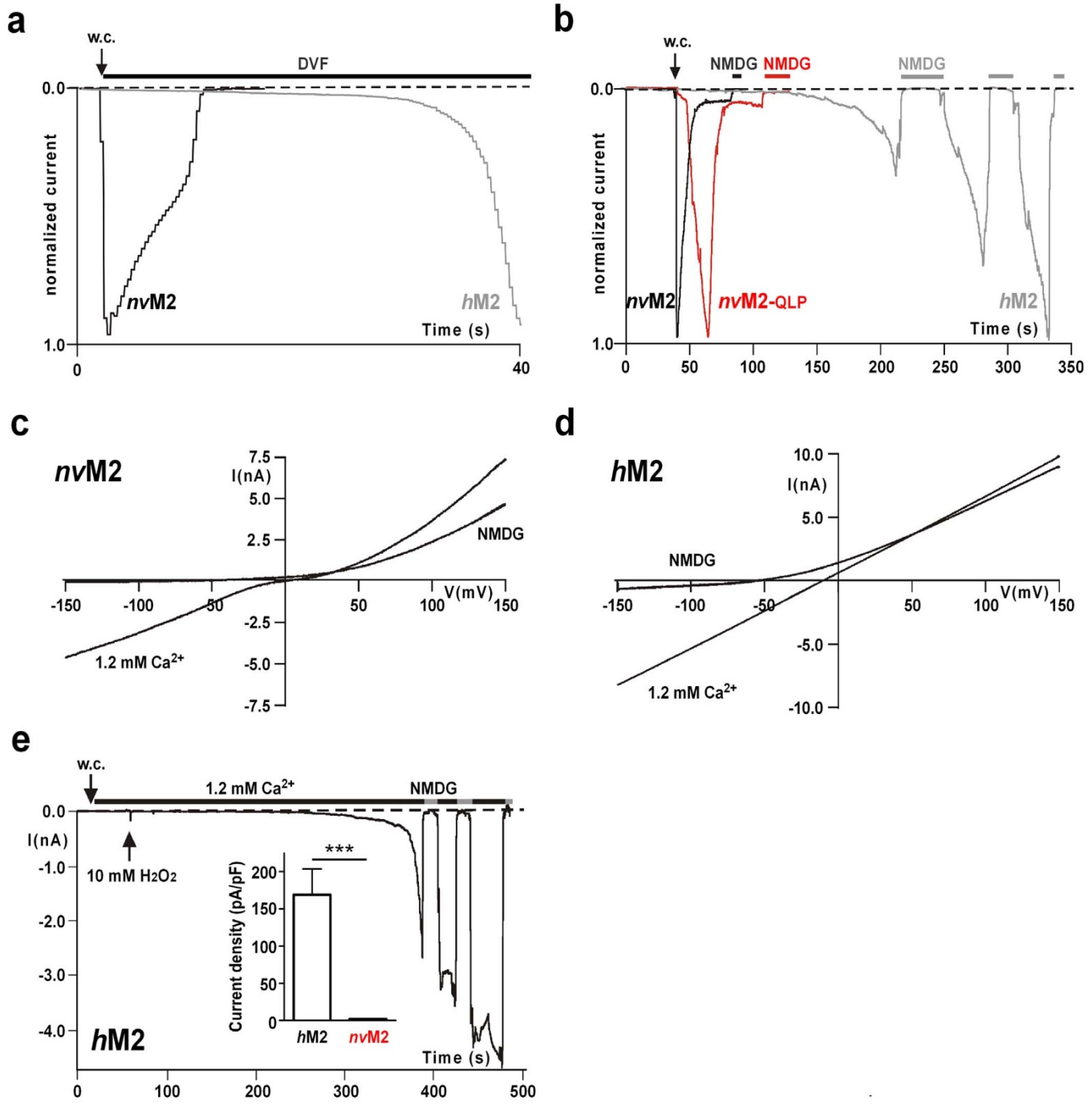

Figure 2 | Current characteristics of *nv*TRPM2, *nv*TRPM2-(QLP) and *h*TRPM2 and sensitivity to H_2O_2. (a) Normalized and superimposed current traces of wild-type *nv*TRPM2 and *h*TRPM2. Each current trace was obtained in a separate experiment by stimulation with ADPR (50 μM) and Ca^{2+} (1 μM) in the pipette solution. The extracellular solution was always divalent free. For each variant similar results were obtained from a least 4 independent experiments. (b) Normalized and superimposed current traces of wild-type *nv*TRPM2, *nv*TRPM2 variant (with pore signature ELF changed to QLP) and *h*TRPM2. Each current trace was obtained in a separate experiment by stimulation with ADPR (100 μM) and ≤10 nM Ca^{2+} in the pipette solution. Currents were initiated by exchanging the extracellular divalent-free solution with standard bath solution containing 1.2 mM Ca^{2+}. Current flow was inhibited by superfusion of the cells with a solution containing NMDG as main cation. For each variant similar results were obtained from a least 5 independent experiments. (c, d) Representative current-voltage relations obtained from whole-cell patch clamp experiments of *nv*TRPM2 (c) and *h*TRPM2 (d). Recordings were performed either in standard bath solution (1.2 mM Ca^{2+}) or in external solution containing NMDG as main cation. (e) Typical current development of *h*TRPM2 during superfusion with standard bath solution containing 10 mM H_2O_2 (time point of application indicated by an arrow). Intracellular concentration of Ca^{2+} was 1 μM. Currents were repeatedly inhibited by NMDG. Data on *h*TRPM2 and *nv*TRPM2 are summarized in the inset figure. ***Indicates a significant difference (P = 0.001) from Student's t-test. *n* = 9–14. Error bars are s.e.

NUDT9H domain, we generated chimeras of *nv*TRPM2 and *h*TRPM2 by exchanging the NUDT9H domains. The swapped NUDT9 sequences (*h*TRPM2: aa 1253–1503; *nv*TRPM2: aa 1289–1551) did not contain the functionally unimportant 60 N-terminal amino acid residues[3]. As a control, we also fused the corresponding part (aa 77–350) of the original *h*NUDT9 enzyme to each channel.

An overview of the structure and the main functional properties of all TRPM2 variants analysed in this study is provided in Figure 3. As expected, the *h*TRPM2 channel variants that received the NUDT9 domain either from *nv*TRPM2 or from the *h*NUDT9 enzyme were inactive (Supplementary Fig. 5; no responses to 0.6 mM ADPR and 1 μM Ca^{2+} in the patch pipette or to extracellular stimulation with 10 mM H_2O_2), in line with previous results in which a partial restoration of the NUDIX consensus motif in *h*TRPM2 was incompatible with channel function[4,5]. By contrast, the *nv*TRPM2 chimera containing the central part of the *h*NUDT9 enzyme (*nv*TRPM2-NUDenz) was functionally indistinguishable from wild-type *nv*TRPM2. This includes the response to ADPR, the insensitivity to H_2O_2, the dependence on Ca^{2+} on at least one side of the cell membrane, as well as the gating kinetics (Fig. 4a–c).

Moreover, the *nv*TRPM2 chimera with the NUDT9H domain of *h*TRPM2 (*nv*TRPM2-*h*NUD) not only responded to ADPR in the same manner as wild-type *nv*TRPM2 (Fig. 4a, d) but had additionally gained sensitivity to H_2O_2 (Fig. 4a, e). HEK-293 cells expressing the *nv*TRPM2-*h*NUD chimera responded with large inward currents upon extracellular stimulation with 10 mM H_2O_2. Again, the activation kinetics were very fast, representing a typical feature of *nv*TRPM2. A quantitative analysis revealed that during the stimulation with 10 mM H_2O_2, the delay between the current onset and a current amplitude of 0.6 nA amounted to 3 ± 1.4 s ($n = 7$). The time over which 90% of the current had declined was 15.5 ± 12 s ($n = 6$). For comparison, the corresponding values for current development in *h*TRPM2 were 116 ± 54 s ($n = 10$; see Figs. 2d and 4e).

Identification of the NUDT9H sequences that confer sensitivity to H_2O_2. In the next step, we narrowed down the sequence requirements for the transfer of the H_2O_2 sensitivity from *h*TRPM2 to *nv*TRPM2. We initially concentrated on the NUDIX box and adjacent sequences. A detailed sequence comparison shows a deletion of a stretch of 14 or 15 amino acid residues slightly downstream of the NUDIX box in *h*TRPM2, compared to the *nv*TRPM2 channel and the *h*NUDT9 enzyme, respectively (Supplementary Fig. 3). Remarkably, this deletion is highly conserved in vertebrate TRPM2- ortholgues but absent in invertebrate TRPM2 channels. Furthermore, *h*TRPM2 contains several arginine residues (R1392, R1400, R1407) within the NUDIX domain where both *nv*TRPM2 and the *h*NUDT9 enzyme have neutral residues instead (Supplementary Fig. 3).

Therefore, we generated single point mutations in *nv*TRPM2 with arginine residues at the relevant positions as well as a *nv*TRPM2 variant with a corresponding deletion of the 15 amino acid residues downstream of the NUDIX box (Supplementary Fig. 3). The corresponding whole-cell patch-clamp data on *nv*TRPM2-(Q1438R) and *nv*TRPM2-(Δ15) are shown in Fig. 5. Similar to wild-type nvTRPM2, both variants displayed similar responses to ADPR as well as current inhibition when Ca^{2+} was removed from both sides of the cell membrane at the same time (Fig. 5a–c). Additionally, the two variants exhibited robust responses to H_2O_2 (Fig. 5a, d, e).

As an additional important finding, the *nv*TRPM2-(Δ15) channel exhibited transient spontaneous currents shortly after breaking into cell (Fig. 5e, f). These currents amounted to 65.2 ± 24 pA/pF, developed exclusively ($n = 9$ vs. $n = 7$ controls) in the presence of intracellular Ca^{2+} (1 μM in the pipette solution) and rapidly returned to baseline (Fig. 5e). The subsequent stimulation with H_2O_2 frequently evoked repetitive current developments that were interrupted by complete returns to baseline (Fig. 5f, $n = 6$ out of $n = 9$ experiments). As an additional control, neither spontaneous currents nor H_2O_2-induced currents were elicited when wild-type *nv*TRPM2 transfected HEK-293 cells were infused with a pipette solution containing 5 μM Ca^{2+} ($n = 7$).

H_2O_2-sensitive *nv*TRPM2 variants induce Ca^{2+}-oscillations in HEK-293 cells. Because the electrophysiological experiments on *nv*TRPM2-(Δ15) revealed that a specific deletion of 15 amino acid residues modifies the *nv*TRPM2 channel from being solely sensitive to ADPR to being additionally sensitive to H_2O_2, we performed calcium imaging experiments with HEK-293 cells transfected either with *nv*TRPM2-(Δ15) or *nv*TRPM2-*h*NUD. The fact that these two *nv*TRPM2 variants can be stimulated by an extracellular stimulus, i.e., H_2O_2, is a prerequisite for this experimental approach.

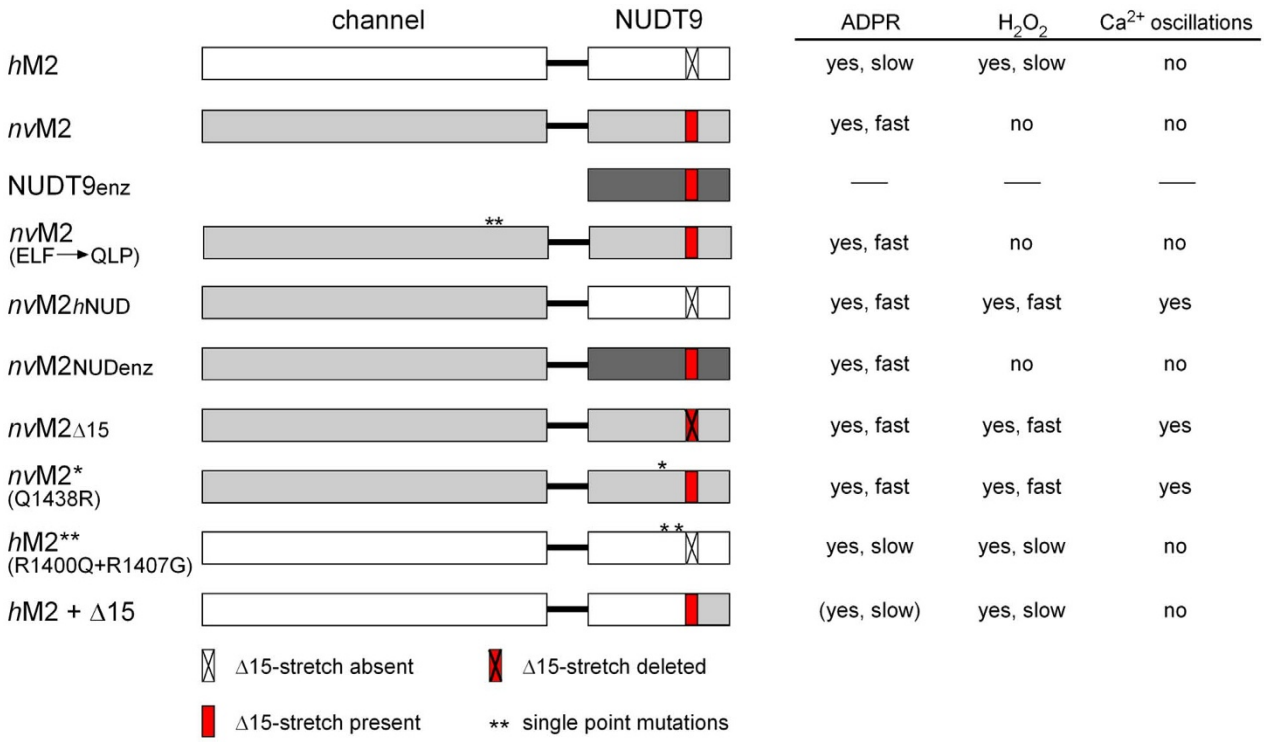

Figure 3 | Overview of all the TRPM2 variants analyzed in this study with schematic representation of their structure and main functional properties.

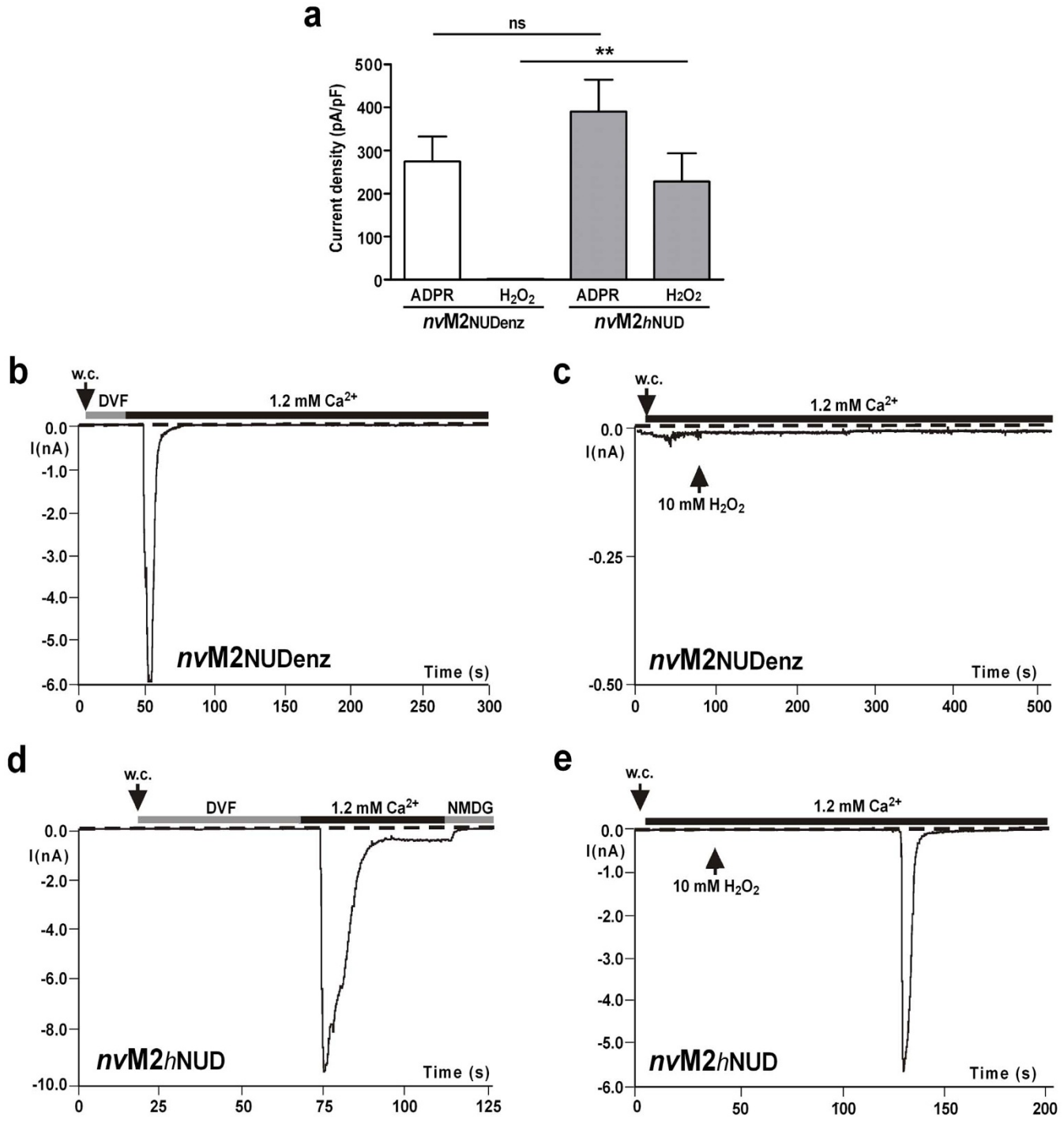

Figure 4 | Sensitivity of *nv*TRPM2 chimeras with alternative NUDT9 domains to intracellular ADPR and extracellular H_2O_2. (a) Average data of whole-cell patch clamp experiments where *nv*TRPM2-NUDenz (*nv*TRPM2 with NUDT9 domain of the *h*NUDT9 enzyme) or *nv*TRPM2-*h*NUD (*nv*TRPM2 with NUDT9 domain of *h*TRPM2) were stimulated either with 50 μM ADPR in the pipette solution (intracellular Ca^{2+}-concentration ≤10 nM) or by extracellular application of 10 mM H_2O_2 (intracellular 1 μM Ca^{2+}). **Indicates a significant difference (P = 0.01) from Student's t-test. n = 5–8. Error bars are s.e. (b)–(e) Representative recordings showing current development of *nv*TRPM2-NUDenz (b, c) and *nv*TRPM2-*h*NUD (d), (e) after stimulation with ADPR or H_2O_2 as indicated. During stimulation with ADPR, the experiments were started in divalent-free bath solution (DVF) and currents only developed after substitution of DVF with standard bath solution with 1.2 mM Ca^{2+}.

As positive control, we used wild-type *h*TRPM2, which showed a consistent and long-lasting increase in $[Ca^{2+}]_i$ in response to H_2O_2 (Fig. 6a) as previously reported (e.g., ref. 27). By contrast, cells transfected with wild-type *nv*TRPM2 showed only a small increase in $[Ca^{2+}]_i$ in response to H_2O_2, which was indistinguishable from those of mock-transfected cells (Fig. 6b–d). In *nv*TRPM2-*h*NUD, a considerable increase in $[Ca^{2+}]_i$ was found after the application of 10 mM H_2O_2 (Fig. 6d, e). Remarkably, rather than a continuous rise in $[Ca^{2+}]_i$, a characteristic oscillation with an intermediate decline of $[Ca^{2+}]_i$ relative to baseline was induced in the continuous presence of H_2O_2 (n = 8 out of 12 cells) (Fig. 6e). Only in *nv*TRPM2-(Δ15) did oscillations in $[Ca^{2+}]_i$ sometimes develop spontaneously (n = 6 out of 19 cells) and were enhanced during stimulation with H_2O_2 (n = 16 out of 19 cells; Fig. 6f). The oscillations in $[Ca^{2+}]_i$ demonstrate the

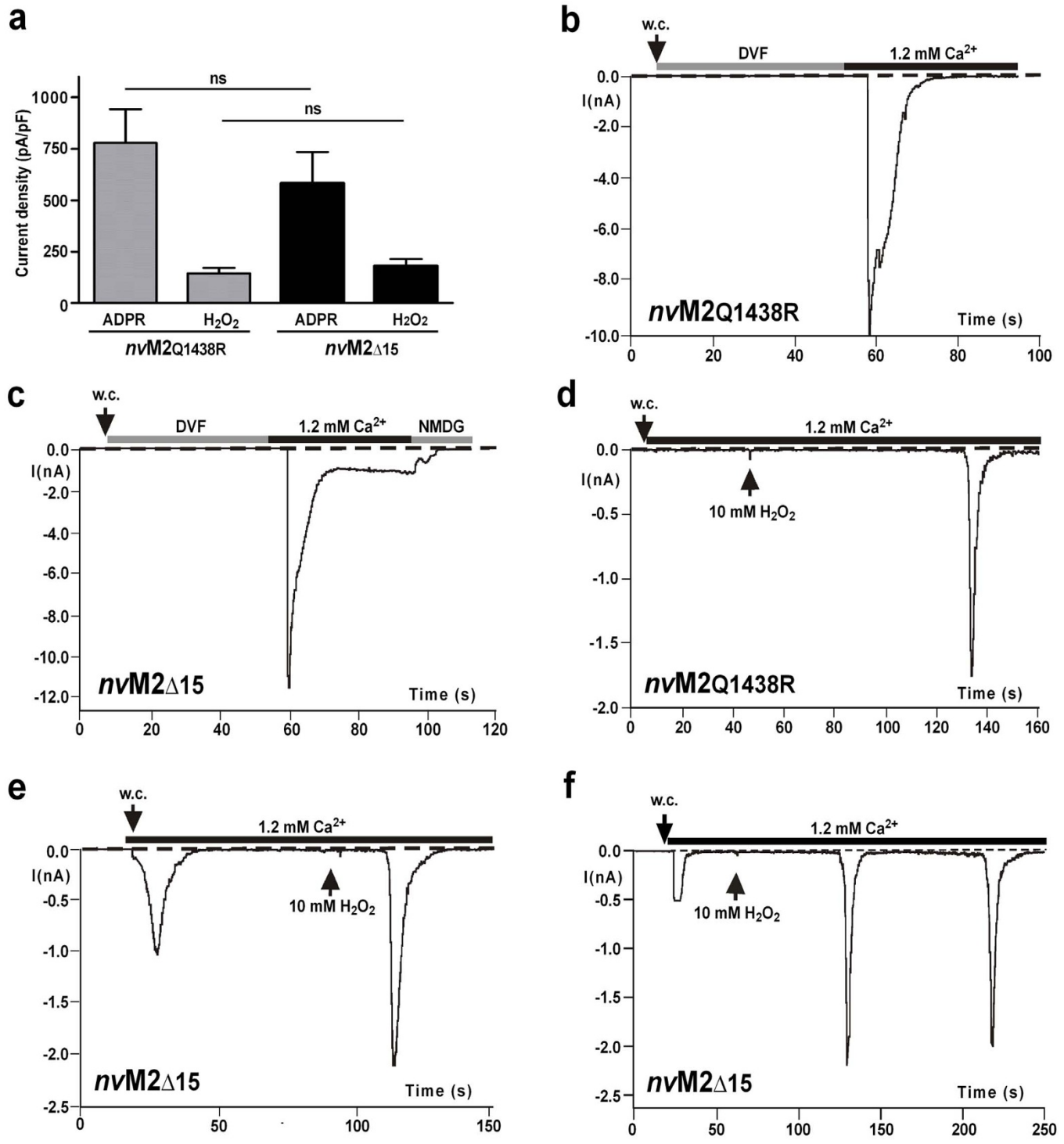

Figure 5 | Sensitivity of *nv*TRPM2 variants with point mutation or deletion within the NUDT9 domain to intracellular ADPR and extracellular H_2O_2. (a) Average data of *nv*TRPM2 variants either containing the point mutation Q1438R or a deletion of a stretch of 15 amino acid residues immediately downstream of the NUDIX box. Stimulation was performed with 50 μM intracellular ADPR or 10 mM extracellular H_2O_2 as described in Fig. 4. $n = 4–9$. (b)–(f) Representative recordings showing current development of *nv*TRPM2-Q1438R and *nv*TRPM2-(Δ15) after stimulation with ADPR (b), (c) or H_2O_2 (d), (e) as indicated. (f) Note the occurrence of spontaneous currents as well as the development of H_2O_2-induced repetitive currents in the variant *nv*TRPM2-(Δ15).

presence of a positive feedback mechanism during the activation of specific *nv*TRPM2 variants that involves repetitive channel activation in the presence of intracellular Ca^{2+}. This mechanism is best explained by a current enhancement by intracellular Ca^{2+}, in line with the electrophysiological data.

Mutation of critical NUDT9H sequences in *h*TRPM2. Because a few adjustments according to the sequence of *h*TRPM2 make the *nv*TRPM2 channel additionally sensitive to H_2O_2, it might be expected that responses to H_2O_2 are abolished or attenuated in the *h*TRPM2 orthologue with the opposite sequence manipulations.

However, the sensitivity of the mutant *h*TRPM2-(R1400Q + R1407G) to H_2O_2 (Fig. 7a) and ADPR (Fig. 7b) as well as the I/V-curve (Fig. 7c) were unchanged, when compared with wild-type *h*TRPM2. As a further modification of *h*TRPM2, we replaced the entire C-terminal NUDT9H sequence downstream from the NUDIX box with the corresponding segment of *nv*TRPM2 (Supplementary Fig. 3). This segment also includes the sequence of 15 amino acid residues that is deleted in wild-type *h*TRPM2 (but not in the *h*NUDT9 enzyme) and is a potential determinant for the sensitivity to H_2O_2 and the additional effects of intracellular Ca^{2+}. The variant *h*TRPM2-(+Δ15), in the presence of 1 μM $[Ca^{2+}]_i$, was as sensitive to H_2O_2 as wild-type *h*TRPM2 (Figs. 7d and 8a). However, the response to ADPR was significantly reduced when the intracellular co-agonist Ca^{2+} was buffered with EGTA to ≤10 nM (Fig. 8a, b). The presence of 1.2 mM ADPR in the pipette solution evoked only small currents in *h*TRPM2-(+Δ15), compared with wild-type *h*TRPM2, which displayed a strong and fast current development at similar concentrations (Fig. 8a, c). By contrast, the currents of *h*TRPM2-(+Δ15) in the presence of 1 μM $[Ca^{2+}]_i$ were similar to those recorderd from *h*TRPM2, even at concentrations as low as 0.15 mM ADPR (Fig. 8a, d).

Discussion

So far, the function of TRPM2 has been studied only with mammalian orthologues, in which its special role as a gateway for Ca^{2+} in the context of oxidative stress-mediated apoptosis was discovered[7,11,26,28]. Here, we have functionally expressed for the first time a TRPM2-like channel from *Nematostella vectensis* in a human cell line. The functional characterisation of this far distant relative of *h*TRPM2 facilitates new insights into the complex gating phenotype of the TRPM2 chanzyme. Currents through *nv*TRPM2 were induced by ADPR, with a greater sensitivity and faster kinetics than in the human orthologue, whereas the modulation provided by intracellular Ca^{2+} was less pronounced. In striking contrast to its effect on *h*TRPM2, the experimental trigger of oxidative stress, H_2O_2, did not have an effect on *nv*TRPM2. Using a chimeric approach, we iden-

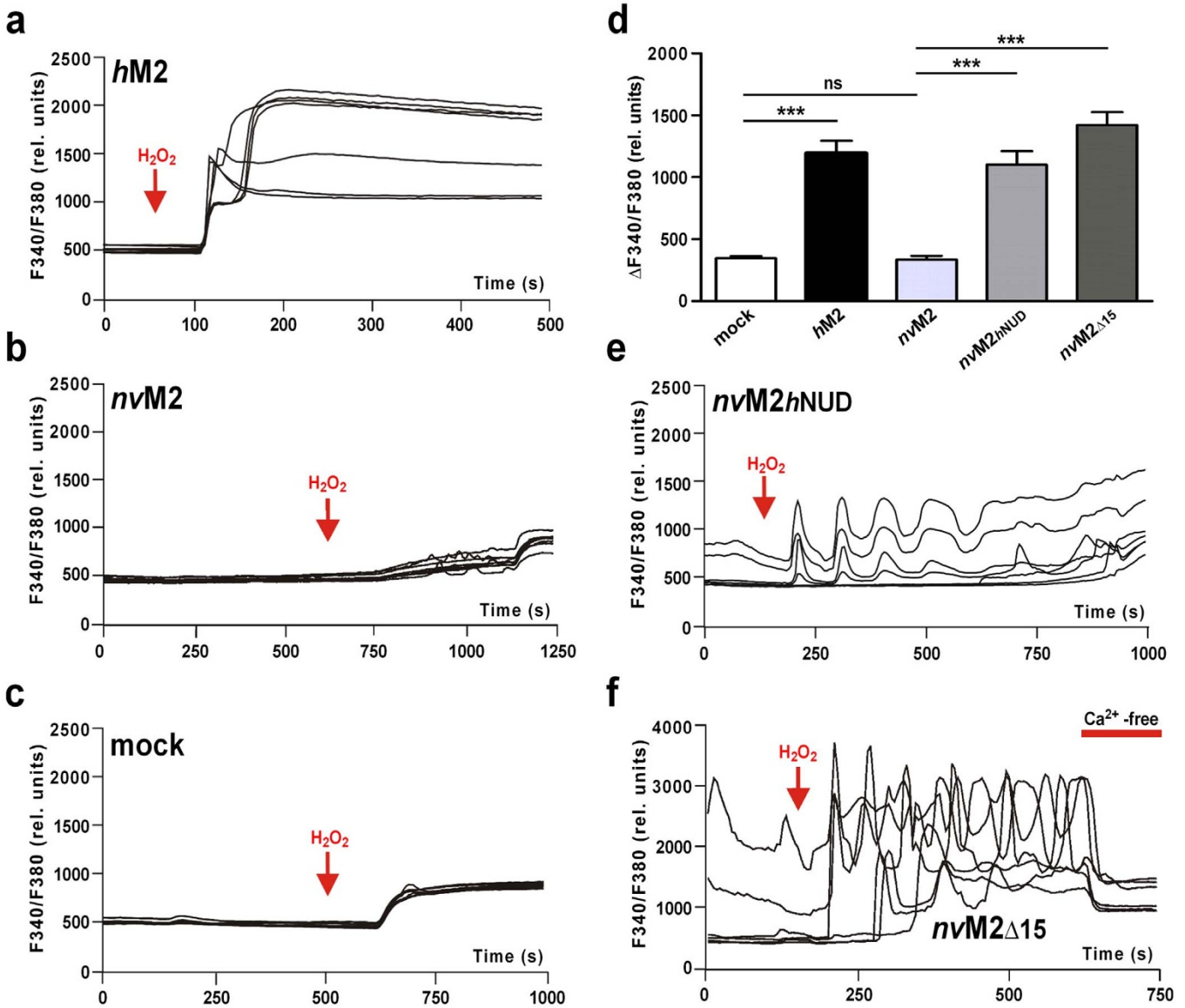

Figure 6 | Activity of H_2O_2-sensitive *nv*TRPM2 variants in measurements of intracellular Ca^{2+} (calcium imaging). (a)–(c), (e), (f) Representative experiments on *h*TRPM2, *nv*TRPM2, empty vector control, *nv*TRPM2-*h*NUD and *nv*TRPM2-(Δ15) as indicated, showing the F340/F380 ratio over time. Extracellular H_2O_2 (10 mM) was added at time points marked with arrows. Maximal increases in F340/F380 are summarized in d. The inhibiting effect of extracellular Ca^{2+} removal is shown in panel f. ***Indicates a significant difference (P = 0.001) evaluated with a one-way ANOVA and the Bonferroni correction. *n* = 12–19. Error bars are s.e.

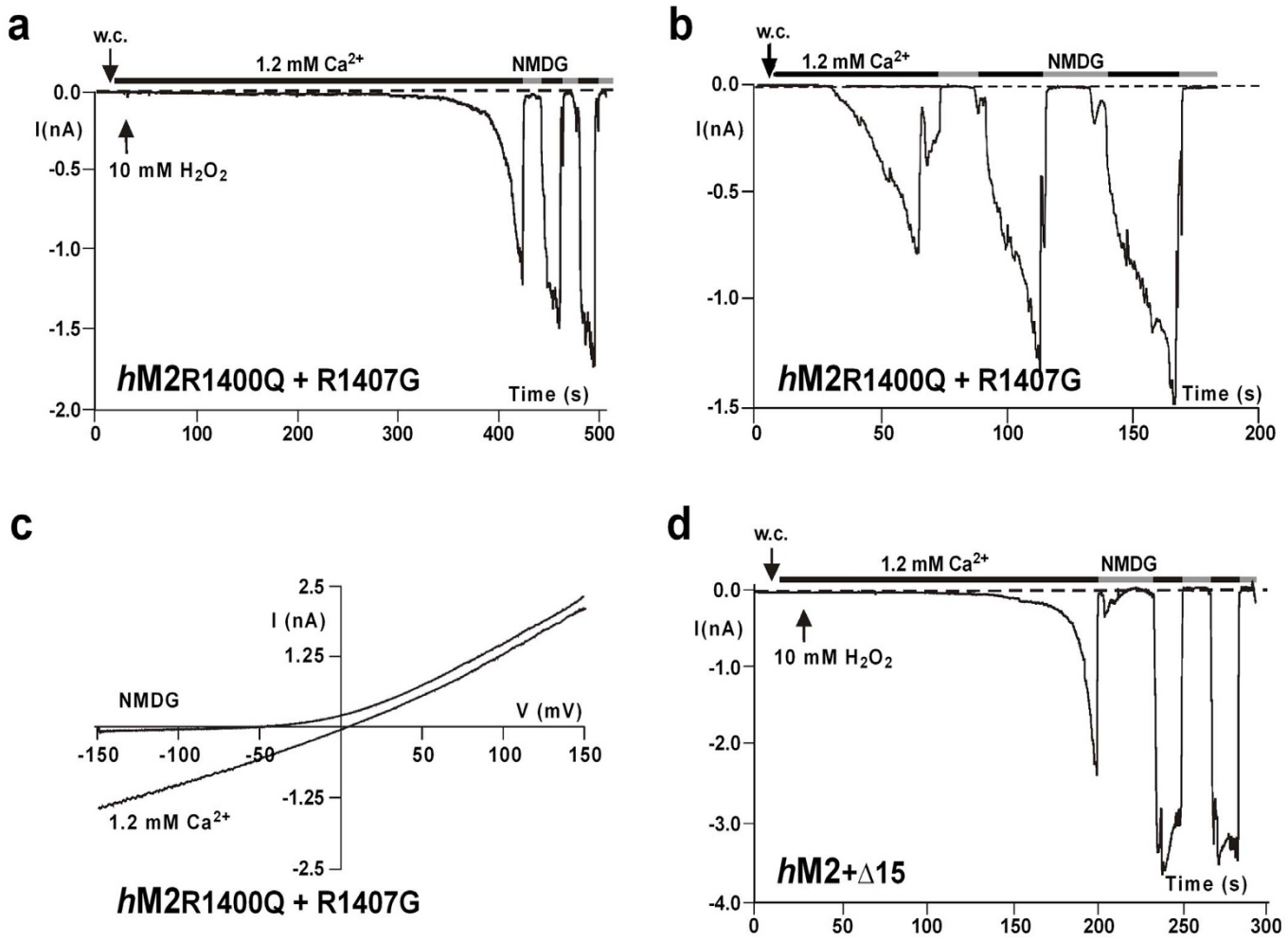

Figure 7 | Sensitivity of *h*TRPM2 variants mutated wihin the NUDT9 domain, to intracellular ADPR and extracellular H_2O_2. (a), (b) Representative whole-cell patch clamp recordings of *h*TRPM2 double mutant R1400Q + R1407G. Stimulation was performed (a) with extracellular 10 mM H_2O_2 or (b) with intracellular 0.3 mM ADPR. (c) Corresponding I/V-relation of currents recorded in panel b. (d) Representative whole-cell patch clamp recording of the variant *h*TRPM2-(+Δ15) that contains the C-terminal part of the NUDT9 domain of *nv*TRPM2 downstream of the NUDIX box. Stimulation was performed with extracellular 10 mM H_2O_2. Currents were repeatedly inhibited by NMDG.

tified some structural elements within the NUDT9 domain that conveyed sensitivity to H_2O_2 and modulated the effects of intracellular Ca^{2+} on *nv*TRPM2 as well as reduced the sensitivity to ADPR in *h*TRPM2. These findings further our understanding of the mechanisms involved in the complex gating process of *h*TRPM2 by various stimuli as well as the adaptions of this cation channel during evolution.

The current view of ADPR as a mediator of oxidative stress-induced apoptosis focuses on the role of mammalian TRPM2 channels as a self-reinforcing gateway of calcium influx[26,28]. It has been suggested that the stimulation of TRPM2 by oxidative stress is indirect, involving an intracellular accumulation of free ADPR[5,25]. Our present findings shed new light on the evolution of sensing oxidative stress because even low intracellular concentrations of ADPR evoke strong and immediate responses in *nv*TRPM2 that are characterised by a short duration, whereas H_2O_2 fails to stimulate the channel. By contrast, *h*TRPM2 has developed into a more polymodal channel with considerably slower kinetics and a distinct modulation by Ca^{2+}. Presumably, the slower kinetics are a prerequisite for the ability of *h*TRPM2 to generate a self-reinforcing and sustained influx of Ca^{2+}, which increases the susceptibility to cell death[11].

Based on a comparative sequence analysis of *h*TRPM2 and *nv*TRPM2, we analysed the effects of the deletion of a stretch of 15 amino acid residues immediately downstream of the NUDIX box as well as the point mutation Q1438R within the NUDIX box. We found that both mutations convey H_2O_2 sensitivity to *nv*TRPM2. As a biological interpretation, by these changes *h*TRPM2 may have developed into a channel responsive to oxidative stress in a more versatile way than *nv*TRPM2 because it reacts to additional and possibly more direct signals than solely to ADPR. These data, especially on the *nv*TRPM2-(Δ15) variant, imply that the sensitivity to H_2O_2 is somehow crucially linked to intracellular Ca^{2+}, but this hypothesis requires extensive future work. It is likely that further genetic alterations with the same effect exist because the reverse changes in *h*TRPM2, i.e., the chimera *h*TRPM2-(+Δ15) and the point mutations R1400Q + R1407G, did not abolish its responses to H_2O_2.

Compared with *h*TRPM2, *nv*TRPM2 exhibits peculiar characteristics especially in the time courses of activation and inactivation. The *h*TRPM2 channel shows on-reactions with a characteristic delay and a gradual development of current, followed by a very slow inactivation. By contrast, the activation of *nv*TRPM2 occurs within a few seconds, after which a clear and rapid inactivation ensues. Importantly, these species-specific kinetics are preserved after all of the manipulations on the NUDT9 domain and additionally applies to the newly acquired H_2O_2 responses of particular *nv*TRPM2 variants. Therefore, it could be hypothesised that the different kinetics do not represent differences in the reactions of the NUDT9 domain

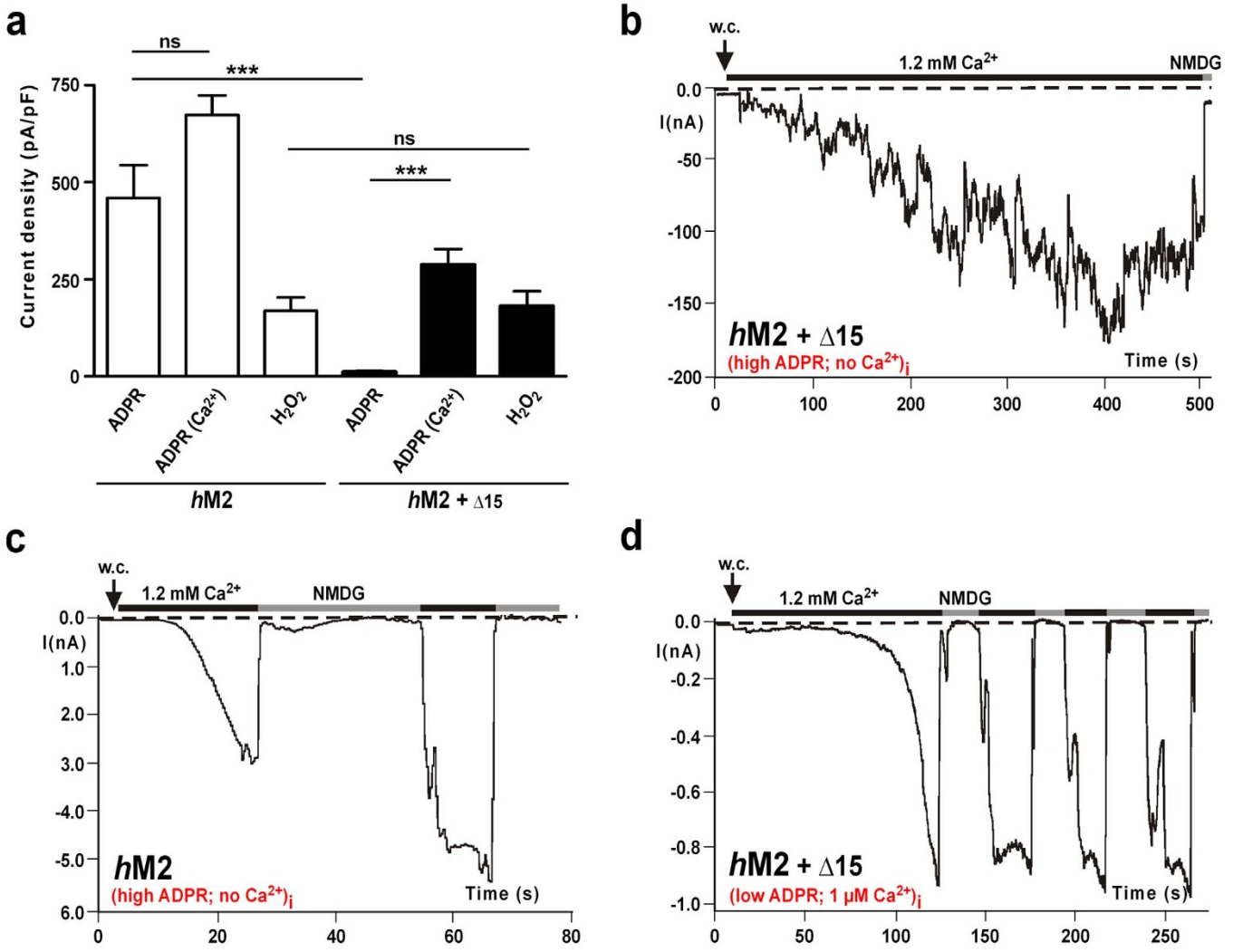

Figure 8 | Sensitivity of the *h*TRPM2 variant *h*TRPM2-(+Δ15) to intracellular ADPR in the presence or absence of intracellular free Ca^{2+}. (a) Average data of wild-type *h*TRPM2 and *h*TRPM2-(+Δ15) under stimulation with either intracellular ADPR (1.2 mM + ≤10 nM $[Ca^{2+}]_i$ or 0.15 mM + 1 μM $[Ca^{2+}]_i$) or extracellular 10 mM H_2O_2. ***Indicates a significant difference (P = 0.001) from Student's t-test. n = 6–11. Error bars are s.e. (b)–(d), Representative whole-cell patch clamp recordings on *h*TRPM2-(+Δ15) and wild-type *h*TRPM2 as indicated, either stimulated with 1.2 mM intracellular ADPR in the presence of ≤10 nM Ca^{2+} in the patch-pipette (b), (c) or with 0.15 mM ADPR in the presence of 1 μM Ca^{2+} in the patch pipette (d).

to the stimuli but rather reflect differences in the mechanisms of how a stimulated NUDT9 domain enables gating of the channel pore. This interactive process of channel gating in TRPM2 remains unclear. Future studies on *nv*TRPM2 may help to improve our understanding of this issue.

A characteristic feature of *h*TRPM2 is its strong dependency on intracellular Ca^{2+} in that there is a dramatic increase in the sensitivity to ADPR by one or two orders of magnitude when $[Ca^{2+}]_i$ is increased from 0 to 1 μM[13,14]. It has been suggested that this makes *h*TRPM2 a mostly $[Ca^{2+}]_i$-regulated channel in the presence of endogenous ADPR levels[24]. The *h*TRPM2 channel possesses at least one potential calmodulin binding domain[29] and the facilitatory effect of $[Ca^{2+}]_i$ was postulated to be mediated by calmodulin[14,29]. However, in *nv*TRPM2 neither the presumed calmodulin binding domain of *h*TRPM2 nor other putative calmodulin binding sites are present. The finding that the channel activation of both *h*TRPM2 and *nv*TRPM2 depends on Ca^{2+}, at least on one side of the cell membrane, strongly suggests that the presumed Ca^{2+} activating sites in the vicinity of the *h*TRPM2 pore[15] are also present in *nv*TRPM2. In line with this idea, our patch-clamp studies on *nv*TRPM2 variants with presumably different permeabilities for Ca^{2+} reveal a significant but relatively small positive feedback of Ca^{2+} on channel activity. So far, these results are compatible with the lack of a calmodulin binding domain in *nv*TRPM2. However, the *nv*TRPM2-(Δ15) variant that contains the specific deletion of 15 amino acid residues characteristic of *h*TRPM2 displayed currents clearly dependent on $[Ca^{2+}]_i$. Moreover, in calcium imaging experiments with HEK-293 cells transfected with *nv*TRPM2-*h*NUD or *nv*TRPM2-(Δ15), oscillations in $[Ca^{2+}]_i$ occurred either spontaneously or after stimulation with H_2O_2. In light of the non-physiological condition of a cnidarian channel chimera in a human expression system, we did not analyse these oscillations in more detail. In any case, because positive as well as negative feedback mechanisms are prerequisites for oscillations, our results provide evidence that the effects of intracellular Ca^{2+} on *nv*TRPM2-(Δ15), even without the binding of calmodulin, are sufficiently strong to create the observed oscillations in $[Ca^{2+}]_i$. The rapid current inactivation of *nv*TRPM2 and its variants is a likely mechanism for the required negative feedback, which is lacking in the human orthologue. In our experiments we did not find any oscillations in $[Ca^{2+}]_i$. for *h*TRPM2. However, Ca^{2+}-oscillations have already been described for TRPM2 endogenously expressed in RIN-5F cells[11], although these observations were obtained under strongly different experimental conditions.

The calcium-imaging data demonstrate that *nv*TRPM2 is inactive in intact cells with physiological concentrations of intracellular ADPR and Ca^{2+}. If the stimulation with extracellular H_2O_2 increased the intracellular level of ADPR, a robust activation should be induced; this was not the case. Moreover, small non-specific rises in $[Ca^{2+}]_i$ induced by extracellular H_2O_2 were not sufficient to stimulate *nv*TRPM2.

The functional properties of *nv*TRPM2-(Δ15) prompted us to create the human variant *h*TRPM2-(+Δ15) that displays a much weaker sensitivity to ADPR than wild-type *h*TRPM2. This is a remarkable feature because reported manipulations of the NUDT9 sequence in *h*TRPM2 have either completely abolished responses to ADPR or left them unaltered[4,5]. Interestingly, the *h*TRPM2-(+Δ15) variant is mutated neither in the putative ADPR binding region nor in the catalytic domain within the NUDIX box, but instead within the C-terminal part of NUDT9. The strongly attenuated response of *h*TRPM2-(+Δ15) to intracellular ADPR was particularly pronounced in the absence of intracellular Ca^{2+}. The presence of Ca^{2+} (1 μM) in the pipette, however, largely restored the ADPR-sensitivity to the wild-type level. These findings with *h*TRPM2-(+Δ15) fit the hypothesis that the affected region is involved in the process that achieves gating of the pore after the binding of ADPR and support the conclusions derived from the different kinetics of *nv*TRPM2 and *h*TRPM2, but this awaits additional experimental studies.

Using several experimental approaches with *nv*TRPM2 variants, we have shown that channel activation by H_2O_2 can be separated from and is not mediated by ADPR. Most strikingly, responses to H_2O_2 were absent in wild-type *nv*TRPM2, although the sensitivity to ADPR is considerably stronger than in *h*TRPM2. Only by making distinct changes in the NUDT9 domain, is sensitivity to H_2O_2 produced, without affecting the ADPR sensitivity. Similarly, the variant *h*TRPM2-(+Δ15) is as sensitive to H_2O_2 as wild-type *h*TRPM2 but responds considerably weaker to ADPR. On the other hand, it is remarkable that the sensitivity to H_2O_2 and the modulatory effects of intracellular Ca^{2+} change in parallel in all variants studied, such that these two activation pathways cannot be discriminated thus far.

We conclude that *h*TRPM2 and its most distant orthologue examined so far, *nv*TRPM2, have been sufficiently conserved during evolution such that *nv*TRPM2 can be functionally expressed in human cells. Moreover, the *nv*TRPM2 channel has been shown to be functionally compatible with the NUDT9 domains of *h*TRPM2 and the *h*NUDT9 enzyme. Recent studies have revealed a striking similarity between *Nematostella vectensis* and vertebrates in terms of genomic organisation and gene content[20,21]. This could be an indication that many fundamental cellular processes of vertebrates and cnidaria were already present in the eumetazoan ancestor. Accordingly, *h*TRPM2 could have evolved from an archaic channel that originally reacted to ADPR in a highly sensitive but temporary manner to one that permits sustained responses. This modification could be a crucial step for the integration of TRPM2 into complex cellular processes. Moreover, by subtle changes within the NUDT9 domain that were partly identified in our experiments, TRPM2 gains sensitivity to H_2O_2 independent of ADPR. Thereby, mammalian TRPM2 channels may respond to an expanded spectrum of messengers and signals of oxidative stress and enable cation influx and enhanced calcium entry.

Methods

Molecular cloning. The amino acid sequence of the TRPM2-like channel of *Nematostella vectensis* was retrieved from the genomic database JGI (http://www.jgi.doe.gov/). The corresponding cDNA (*nv*TRPM2; jgi.Nemve1.248535|estExt_fgenesh1_pg.C_6220005) was synthesized by MWG-Biotech (Ebersberg, Germany) as two independent fragments. The 5′-terminal fragment of 2939 bp starts with a restriction site for *Asc* I followed by the Kozak sequence *gccacc* and the start codon and ends with a restriction site for *Hind* III. The 3′-terminal fragment of 1743 bp starts with the *Hind* III restriction site and ends with a stop codon followed by a *Xba* I restriction site. The codon usage was adapted during synthesis to ensure optimal expression in HEK-293 cells and the DNA sequence (Supplementary Fig. 1) was verified by double-strand DNA sequencing by MWG-Biotech. The 5′-terminal fragment was subcloned via *Asc* I + *Hind* III into the modified pIRES-hrGFP-2a vector (Stratagene, La Jolla, CA, USA) that contains a unique *Asc* I site instead of a single *Nhe* I site as well as a unique *Xba* I site instead of a single *Xho* I site. Subsequently, the 3′-terminal fragment was added via a *Hind* III + *Xba* I cloning step. The cDNA of *h*TRPM2 was subcloned via *Eco* RI + *Xba* I into the pIRES-hrGFP-2a vector. The cDNA from the human NUDT9 enzyme (Accession No: NM_024047.3) was purchased from AMS Biotechnology, (Abingdon, UK). Site-directed mutagenesis was performed using the QuikChange mutagenesis system (Stratagene, La Jolla, CA, USA). Defined oligonucleotides were obtained from MWG-Biotech. Each point mutation and chimeric channel construct was verified by DNA sequencing (MWG-Biotech). All procedures were performed in accordance to the respective manufacturer's instructions, unless indicated otherwise. Sequence alignments were performed according to the UniProtKB alignment tool at www.uniprot.org.

Cell culture and transfection. HEK-293 cells were obtained from the German Collection of Microorganisms and Cell Cultures (Braunschweig, Germany) and cultured in DMEM media (Biochrome, Berlin, Germany) supplemented with 4 mM L-glutamine and 10% (v/v) foetal calf serum (Biochrome) and 2 mM sodium pyruvate. Transient transfections of HEK-293 cells with the cDNAs of *h*TRPM2, *nv*TRPM2 or chimeric variants were performed using the FuGene 6 transfection reagent (Roche, Mannheim, Germany) according to the manufacturer's instructions. As controls, cells were transfected with the pIRES-hrGFP-2a vector alone. The transfected cells were maintained for 24 h in an incubator at 37°C and 5% CO_2. Subsequently, the cells were seeded on poly-lysine-coated glass coverslips at a suitable dilution and further incubated for 3–4 h. Then, patch-clamp and calcium imaging experiments were carried out in cells visibly positive for EGFP. At least three independent transfections were used for each experimental group.

Electrophysiology. Whole-cell recordings were performed using an EPC 9 amplifier equipped with a personal computer with Pulse 8.5 and X Chart software (HEKA, Lamprecht, Germany). The standard bath solution contained (in mM) 140 NaCl, 1.2 $MgCl_2$, 1.2 $CaCl_2$, 5 KCl, 10 HEPES, pH 7.4 (NaOH). For Na^+ free solutions, Na^+ was replaced by 150 mM N-methyl-D-glucamine (NMDG) and the titration was performed with HCl. The divalent free bath solution (DVF) contained (in mM) 150 NaCl, 10 EGTA, 10 HEPES, pH 7.4 (NaOH). The pipette solution contained (in mM) 145 CsCl, 8 NaCl, 2 $MgCl_2$, 10 HEPES, pH 7.2 (CsOH) and the Ca^{2+} concentration was adjusted to either ≤10 nM (10 mM Cs-EGTA, no Ca^{2+} addition), to 1 μM (0.886 mM Ca^{2+}, 1 mM Cs-EGTA) or to 5 μM (0.970 mM Ca^{2+}, 1 mM Cs-EGTA). The Ca^{2+} concentration of the solutions was calculated using the *MAXC*-program: (http://www.stanford.edu/~cpatton/maxc.html). For the stimulation of TRPM2, Adenosine diphosphate ribose (ADPR; 100 mM stock solution in distilled water) was added to the intracellular solution yielding a final concentration of 0.001-1.2 mM. Alternatively, TRPM2 currents were evoked by superfusion of the cells with standard bath solution containing 10 mM H_2O_2 (diluted from a 30% stock solution). Unless otherwise stated, the experiments were performed at room temperature (21°C) and the current-voltage relations were obtained during voltage ramps from −150 to +150 mV and back to −150 mV applied over 200 ms. The holding potential was −60 mV. For the analysis the maximal current amplitudes (pA) in a cell were divided by the cell capacitance (pF), a measure of the cell surface. The result is the current density (pA/pF).

Calcium imaging experiments. For fluorescence imaging of $[Ca^{2+}]_i$ HEK-293 cells on poly-lysine-coated glass coverslips were loaded in standard bath solution containing membrane-permeable Fura-2 acetoxymethyl ester (1.5 ng/μl; Invitrogen) and pluronic acid (0,025%) for 20 min at 37°C. Fluorescence was alternately excited at 340 and 380 nm using the Polychrome IV monochromator (TILL Photonics). The emitted fluorescence was measured at 510 nm using a Sensicam (IMAGO). Fluorescence was corrected for background at each wavelength. Measurements were obtained at room temperature (21°C). The standard bath solution and stimulation with H_2O_2 were identical to those described for the patch-clamp experiments.

Data analysis and statistics. Data are expressed as the mean ± s.e.m.. Unless statet otherwise, the comparison of two groups was performed using an unpaired Student's t-test. Calcium imaging experiments were statistically evaluated using a one-way ANOVA and the Bonferroni correction was applied when multiple comparisons were performed with the same control data. Differences were considered significant at $^{**}P < 0.01$ and $^{***}P < 0.001$.

1. Perraud, A. L. *et al.* ADP-ribose gating of the calcium-permeable LTRPC2 channel revealed by Nudix motif homology. *Nature* **31**, 595–599 (2001).
2. Ribeiro, J. M., Carloto, A., Costas, M. J. & Cameselle, J. C. Human placenta hydrolases active on free ADP-ribose: an ADP-sugar pyrophosphatase and a specific ADP-ribose pyrophosphatase. *Biochim Biophys Acta.* **1526**, 86–94 (2001).
3. Shen, B. W., Perraud, A. L., Scharenberg, A. & Stoddard, B. L. The crystal structure and mutational analysis of human NUDT9. *J Mol Biol.* **332**, 385–398 (2003).
4. Kühn, F. J. & Lückhoff, A. Sites of the NUDT9-H domain critical for ADP-ribose activation of the cation channel TRPM2. *J Biol Chem.* **279**, 46431–46437 (2004).

5. Perraud, A. L. *et al.* Accumulation of free ADP-ribose from mitochondria mediates oxidative stress-induced gating of TRPM2 cation channels. *J Biol Chem.* **280**, 6138–6148 (2005).
6. Howard, M. *et al.* Formation and hydrolysis of cyclic ADP-ribose catalyzed by lymphocyte antigen CD38. *Science* **262**, 1056–1059 (1993).
7. Fonfria, E. *et al.* TRPM2 channel opening in response to oxidative stress is dependent on activation of poly(ADP-ribose) polymerase. *Br J Pharmacol.* **143**, 186–192 (2004).
8. Buelow, B., Song, Y. & Scharenberg, A. M. The Poly(ADP-ribose) polymerase PARP-1 is required for oxidative stress-induced TRPM2 activation in lymphocytes. *J Biol Chem.* **283**, 24571–24583 (2008).
9. Faouzi, M. & Penner, R. TRPM2. *Handb Exp Pharmacol.* **222**, 403–426 (2014).
10. Ru, X. & Yao, X. TRPM2: a multifunctional ion channel for oxidative stress sensing. *Sheng Li Xue Bao.* **66**, 7–15 (2014).
11. Hara, Y. *et al.* LTRPC2 Ca^{2+}-permeable channel activated by changes in redox status confers susceptibility to cell death. *Mol Cell.* **9**, 163–173 (2002).
12. Wehage, E. *et al.* Activation of the cation channel long transient receptor potential channel 2 (LTRPC2) by hydrogen peroxide. A splice variant reveals a mode of activation independent of ADP-ribose. *J Biol Chem.* **277**, 23150–23156 (2002).
13. McHugh, D., Flemming, R., Xu, S. Z., Perraud, A. L. & Beech, D. J. Critical intracellular Ca^{2+} dependence of transient receptor potential melastatin 2 (TRPM2) cation channel activation. *J Biol Chem.* **278**, 11002–11006 (2003).
14. Starkus, J., Beck, A., Fleig, A. & Penner, R. Regulation of TRPM2 by extra- and intracellular calcium. *J Gen Physiol.* **130**, 427–440 (2007).
15. Csanády, L. & Törocsik, B. Four Ca^{2+} ions activate TRPM2 channels by binding in deep crevices near the pore but intracellularly of the gate. *J Gen Physiol.* **133**, 189–203 (2009).
16. Gracheva, E. O. *et al.* Molecular basis of infrared detection by snakes. *Nature* **464**, 1006–1011 (2010).
17. Mederos, Y., Schnitzler, M., Wäring, J., Gudermann, T. & Chubanov, V. Evolutionary determinants of divergent calcium selectivity of TRPM channels. *FASEB J.* **22**, 1540–1551 (2007).
18. Nakanishi, N., Renfer, E., Technau, U. & Rentzsch, F. Nervous systems of the sea anemone Nematostella vectensis are generated by ectoderm and endoderm and shaped by distinct mechanisms. *Development* **139**, 347–357 (2012).
19. Miller, D. J. *et al.* The innate immune repertoire in cnidaria--ancestral complexity and stochastic gene loss. *Genome Biol.* **8**, R59 (2007).
20. Putnam, N. H. *et al.* Sea anemone genome reveals ancestral eumetazoan gene repertoire and genomic organization. *Science* **317**, 86–94 (2007).
21. Darling, J. A. *et al.* Rising starlet: the starlet sea anemone, Nematostella vectensis. *Bioessays* **27**, 211–221 (2005).
22. Ikemura, T. Codon usage and tRNA content in unicellular and multicellular organisms. *Mol Biol Evol.* **2**, 13–34 (1985).
23. Bessman, M. J., Frick, D. N. & O'Handley, S. F. The MutT proteins or "Nudix" hydrolases, a family of versatile, widely distributed, "housecleaning" enzymes. *J Biol Chem.* **271**, 25059–25062 (1996).
24. Heiner, I. *et al.* Endogenous ADP-ribose enables calcium-regulated cation currents through TRPM2 channels in neutrophil granulocytes. *Biochem J.* **398**, 225–32 (2006).
25. Tóth, B. & Csanády, L. Identification of direct and indirect effectors of the transient receptor potential melastatin 2 (TRPM2) cation channel. *J Biol Chem.* **285**, 30091–30102 (2010).
26. Kashio, M. *et al.* Redox signal-mediated sensitization of transient receptor potential melastatin 2 (TRPM2) to temperature affects macrophage functions. *Proc Natl Acad Sci U S A* **109**, 6745–6750 (2012).
27. Hecquet, C. M., Ahmmed, G. U., Vogel, S. M. & Malik, A. B. Role of TRPM2 channel in mediating H_2O_2-induced Ca^{2+} entry and endothelial hyperpermeability. *Circ Res.* **102**, 347–355 (2007).
28. Park, L. *et al.* The key role of transient receptor potential melastatin-2 channels in amyloid-β-induced neurovascular dysfunction. *Nat Commun.* **5**, 5318. doi: 10.1038/ncomms6318 (2014).
29. Tong, Q. *et al.* Regulation of the transient receptor potential channel TRPM2 by the Ca^{2+} sensor calmodulin. *J Biol Chem.* **281**, 9076–9085 (2006).

Acknowledgments

We thank Daniel C. Hoffmann and Marina Wolf for their help during the course of this study. The study was supported by the Deutsche Forschungsgemeinschaft (DFG KU 2271/4-1).

Author contributions

F.K. developed the concept, designed the study, performed all whole-cell patch clamp experiments, analysed the data and wrote the paper. C.K. conducted all calcium imaging experiments and analysed the data. A.L. was involved in data interpretation and preparing of the manuscript. All authors discussed the results and implications and commented on the manuscript at all stages.

Additional information

Supplementary information accompanies this paper at http://www.nature.com/scientificreports

Competing financial interests: The authors declare no competing financial interests.

How to cite this article: Kühn, F.J.P., Kühn, C. & Lückhoff, A. Functional Characterisation of a TRPM2 orthologue from the sea anemone *Nematostella vectensis* in human cells. *Sci. Rep.* **5**, 8032; DOI:10.1038/srep08032 (2015).